International Journal of Hydrogen Energy 114 (2025) 267–278

Contents lists available at ScienceDirect

International Journal of Hydrogen Energy

journal homepage: www.elsevier.com/locate/he

Molecular study of high-pressure hydrogen decompression in amorphous polyethylene

Guozhen Ding [a], Christopher J. Tighe [b], Lik-ho Tam [c,*], Chao Wu [a,**]

[a] Department of Civil and Environmental Engineering, Imperial College London, South Kensington Campus, Imperial College Road, London, SW7 2AZ, UK
[b] Department of Chemical Engineering, Imperial College London, South Kensington Campus, Imperial College Road, London, SW7 2AZ, UK
[c] School of Transportation Science and Engineering, Beihang University, 37 Xueyuan Road, Beijing, 100191, China

ARTICLE INFO

Handling Editor: Dr. E.C. Kumbur

Keywords:
Hydrogen storage tank
Polyethylene liner
Rapid decompression failure
Molecular dynamics
Hydrogen solubility

ABSTRACT

Polyethylene (PE) is widely used as a liner material in high-pressure composite hydrogen storage tanks. During routine operation or maintenance, gas decompression occurs, resulting in pressure differentials within the polymer that lead to degradation or even failure if the rate of decompression is too high. Therefore, a comprehensive, fundamental understanding of the failure mechanisms of PE during rapid decompression is important to guide the development of safe operating procedures. In this study, atomistic simulations are employed to investigate the microstructural changes in amorphous PE during rapid decompression, under the influence of pressure, temperature, and stress. It is shown that the solubility of hydrogen in amorphous PE increases with both temperature and pressure, as observed in experimental work in the prior literature, exhibiting dual-mode sorption behaviour above the glass transition temperature. As decompression starts, the fractional free volume (FFV) within PE is observed to increase, with a corresponding increase in the number and size of free volume pores; it is hypothesised that this signifies the onset of cavitation damage. An increase in hydrogen content and initial pressure significantly increases free volume generation druing decompression, thereby increasing the risk of cavitation. Higher temperatures and tensile stresses also contribute to an increase in free volume generation. On a molecular level, the mechanism of rapid decompression involves volumetric expansion, leading to increased internal free volume, with hydrogen molecules further facilitating free volume generation. These molecular insights contribute to a deeper understanding of the failure mechanisms of PE, helping predict material degradation and failure during high-pressure hydrogen decompression.

1. Introduction

The pursuit of a sustainable energy future necessitates a transition away from fossil fuel-based energy sources towards clean and renewable alternatives. Among these, hydrogen has emerged as a frontrunner due to its remarkable energy density (per unit mass), versatility, and environmental benefits [1]. However, the low density and high diffusivity of hydrogen pose severe challenges for its storage and transportation [2–5]. To achieve efficient storage and transport, hydrogen can be compressed to high pressures [6–8]. Under such extreme conditions, hydrogen storage materials must possess excellent mechanical strength, gas barrier properties, and long-term chemical stability. Traditional metal hydrogen storage tanks are heavy and prone to hydrogen embrittlement, while polymer materials have become a research focus due to their light weight, corrosion resistance, ease of processing, and immunity to hydrogen embrittlement [9]. Type IV hydrogen storage tanks, as shown in Fig. 1(a), are composite pressure vessels primarily constructed from polymeric materials. They provide a significant advancement in hydrogen storage technology and address many limitations of traditional metal tanks. These hydrogen storage tanks consist of a polymer liner, typically made from materials such as high-density polyethylene (HDPE), encased in a carbon fibre reinforced polymer shell [10]. During the operation of Type IV hydrogen storage tanks, hydrogen molecules penetrate and occupy existing cavities or gaps within the polymeric materials. When the tank experiences rapid decompression, the diffusion rate of hydrogen molecules within the material cavities is slower than the decompression rate. Inadequate diffusion time within the cavities leads to a pressure differential inside

* Corresponding author.
** Corresponding author.
E-mail addresses: leo_tam@buaa.edu.cn (L.-h. Tam), c.wu@imperial.ac.uk (C. Wu).

https://doi.org/10.1016/j.ijhydene.2025.03.056
Received 6 December 2024; Accepted 3 March 2025
Available online 7 March 2025
0360-3199/© 2025 The Author(s). Published by Elsevier Ltd on behalf of Hydrogen Energy Publications LLC. This is an open access article under the CC BY license (http://creativecommons.org/licenses/by/4.0/).

the material (higher internally, lower externally). When the internal hydrogen pressure within the cavities exceeds the yield strength of the polymeric materials, hydrogen molecules in the material enlarge the cavities within which they are trapped, causing the inner liner to blister or even crack. Furthermore, permeation of hydrogen results in its accumulation in the space between the inner liner and the outer composite material layer of the tank; this causes the pressurisation of this gap, which may in turn lead to the complete collapse of the liner when the tank is depressurised. This type of failure, referred to as rapid decompression failure, typically occurs in extreme situations such as uncontrolled loss of containment (e.g. due to component damage), routine inspections, and aging tests [11]. Thus failure of the polymer on decompression can occur on several length scales, categorized into three distinct modes[12–14]: buckling (collapse of the liner), blistering (localized macroscopic flaws), and cavitation (microscopic cavity formation). Predicting the onset of cavitation failure, depicted in Fig. 1(b), is the focus of this work. Fig. 1(c) depicts molecules of hydrogen gas dissolved in PE at the nanoscale, showing regions of free volume within the polymer structure.

Historically, researchers have extensively used experimental methods to explore rapid decompression failure, with the focus on understanding the mechanisms of the impact of various factors on material performance in hydrogen storage systems. Previous studies have investigated how the intrinsic properties of polymer materials, such as mechanical and diffusion properties, as well as crystallinity, influence their behaviour under rapid decompression. Specifically, it has been shown that HDPE typically suffers more severe damage from rapid decompression compared to polyamide (PA), which can be attributed to PA having a higher yield strength and lower solubility of H_2 [15,16]. Experimental studies have shown that polymers with lower crystallinity exhibit more severe damage during rapid decompression, primarily occurring in the amorphous regions where hydrogen gas dissolves [11, 17,18]. This trend may be caused by the suppression of H_2 solubility in the amorphous regions by interactions with the crystallites, e.g. via tie chains [19]; this reduces gas accumulation in the amorphous regions and, consequently, lowers susceptibility to damage. Such interactions with the crystalline regions may also help to mechanically stabilize the amorphous polymer thus reducing damage induced by rapid decompression. Apart from the intrinsic properties of the material, external operating conditions (such as temperature, pressure, decompression rate, and gas charging/discharging cycles) also significantly impact rapid decompression failure, e.g. with the propensity to failure increasing at higher temperatures [20–23]. Hydrogen decompression tests on 700 atm pressure vessel prototypes, filled to 50% or 100% capacity and vented with flow rates up to 7 atm/min, have demonstrated that higher initial pressures and faster decompression rates lead to more significant collapse of the liner [24]. Observations of HDPE and PA after decompression periods of 1, 3, 5, and 13 h indicate that shorter decompression durations result in greater decompression-induced cavitation damage [16]. In service, hydrogen storage tanks undergo multiple hydrogen charging and discharging cycles, during which damage gradually accumulates. A quantitative method has been developed, to assess bulk damage levels in polymeric materials after exposure to high-pressure hydrogen [25]. HDPE specimens subjected to 900 atm hydrogen cycles were used to quantify internal damage via transmitted light brightness and relative extinction ratio. A logarithmic increase in transmitted light intensity with the number of exposure cycles was observed, which indicated increased internal damage. Transmission electron microscopy (TEM) observations of the early stages of cavitation in polyvinylidene fluoride (PVDF) showed that hydrogen gas decompression leads to the formation of cavities measuring 2–3 nm in diameter [26]. These observations highlight the significance of gas decompression in initiating cavitation at the nanoscale.

Although experimental methods shed light on the conditions under which rapid decompression damage is more likely to occur, they do not give much insight into the fundamental mechanism that initiates cavitation and blistering damage in particular. Simulation methods can provide in-depth analysis of the initiation and evolution of material damage, so that they can provide a deeper insight into rapid decompression failure and predict material failure under extreme conditions. A numerical model was developed to understand plastic liner cavitation during decompression [16]. Based on a hydrogen solubility derived from Henry's law and non-steady state diffusion described by Fick's second law, this model accurately predicted the onset of cavitation by considering liner thickness and decompression rate. Building on this foundational work, a method utilizing non-dimensional parameters was introduced to assess cavitation risk [12]. The numerical results were validated against existing literature on cavitation in polymers. Finite element modelling was also used to predict damage during rapid decompression of ethylene propylene diene terpolymer (EPDM) at the mesoscale [13,27]. The effects of fillers and plasticizers on damage were studied. Meanwhile, damage evolution in the presence of multiple cavities was explored, which revealed a change in the damage propagation path due to stress field interactions. It was also found that a simple diffusion model could not adequately explain hydrogen gas release kinetics in nitrile butadiene rubber (NBR) composites under high pressure [28]. To address this, a phase field model was developed, considering defect-enhanced evolution of hydrogen gas bubbles and concentration-dependent diffusivity of the hydrogen [28]. This model accurately described experimentally-measured kinetics of H_2 desorption, predicting the onset of gas bubble evolution and degradation in material properties. The current simulation approaches have advanced the understanding of rapid decompression failure mechanisms, such as damage initiation, cavitation risk, and mesoscale interactions. However, the detailed progression of damage from nano-scale phenomena to macro-scale material failure remains unclear. This limitation poses a

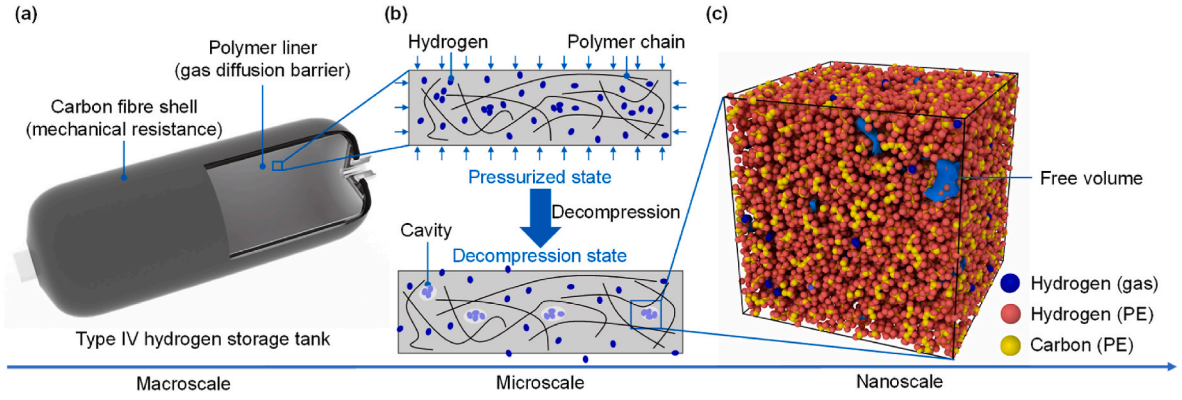


Fig. 1. Schematic diagram of rapid decompression: (a) type IV hydrogen storage tank, (b) microscopic cavitation, and (c) molecular model consisting of PE chains and hydrogen molecules from this work.

challenge for accurately predicting the overall failure process, as current simulation methods may not fully capture the multi-scale interactions involved.

Recent efforts have been made to comprehend rapid decompression failure at a micro-scale using molecular dynamics (MD) simulations. MD simulations are an effective tool for addressing these issues, as they provide detailed insights into the atomistic-level interactions and dynamics that drive these phenomena. The molecular restructuring of EPDM with various crosslink densities during rapid decompression has been investigated [29]. It was noted that while higher crosslink density reduces volumetric expansion, it also introduces potential sites for the local clustering of gas molecules, which are precursors to cavitation-induced failure. The behaviour of PE in a hydrogen environment has been investigated using all-atom MD simulations [10]. The findings suggest that rapid decompression leads to the aggregation of hydrogen molecules into nano-sized bubbles within the polymer matrix. These bubbles form and dissipate during drops in pressure and remain stable only at very low pressures. Furthermore, MD simulations have been employed to explore the effects of hydrogen and pressure on the physical and tensile properties of amorphous PE [30]. It is found that while hydrogen weakens molecular interactions and reduces tensile properties, pressure enhances tensile properties by increasing trans conformations and molecular orientation when exposed to high-pressure hydrogen [30]. Cavitation-induced damage is found to emerge from nano-scale phenomena such as molecular rearrangement, stress induction during localized gas accumulation, and eventual fracture through chain scission [31]. However, current molecular-scale computational studies lack a complete understanding of rapid decompression failure mechanisms, including atomistic interactions, molecular rearrangements, and hydrogen-induced cavitation, which impedes the fundamental understanding of material behaviour under rapid decompression.

This study focuses on the early stages of cavitation induced by rapid decompression. Experimental observations have revealed the formation of nanometre-scale cavities [26], which are likely to originate from the generation and aggregation of sub-nanometre-scale free volume. To investigate this phenomenon, atomistic molecular dynamics simulations are employed to explore the molecular behaviour of amorphous polyethylene (PE) during decompression from an initially high hydrogen pressure and to uncover the underlying mechanisms. First, molecular models of amorphous PE are constructed. Grand canonical Monte Carlo (GCMC) simulations are used to determine the solubility of hydrogen molecules within the PE system at different initial pressures and temperatures. These models are then subjected to simulations of rapid gas decompression. The evolution of free volume is measured to quantify the risk of cavitation damage caused by rapid decompression, hypothesizing that free volume generation represents the initial stage of cavitation in amorphous PE. The effects of various factors are discussed, including initial pressure, temperature, and stress, on the decompression process. The simulation results reported in this study provide insights into the nanoscale behaviour of PE under high-pressure hydrogen decompression conditions, which contributes to a comprehensive understanding and ability to predict the failure of polymer liners.

2. Computational methods

2.1. Atomistic model and molecular interactions

First, three all-atom amorphous PE models with a density of 0.85 g•cm^{-3} are generated and geometrically optimized [32]. The use of three models aims to repeat the simulations to ensure sufficient sampling to capture structural variability and improve statistical reliability of the results. The use of amorphous models in this study is justified by the fact that rapid decompression failure predominantly occurs in the amorphous regions of polymers, where hydrogen molecules primarily dissolve [17]. In addition, the effect of the crystallites on depressing solubility in the amorphous region [19] is neglected, thus the predictions of the model will be conservative for semicrystalline polymers. The three-dimensional periodic PE model contains 20 PE chains, each comprising 250 monomers (C_2H_2), which results in simulation cells of approximate size 6.5 × 6.5 × 6.5 nm^3, as shown in Fig. 1(c). The choice of chain length and the number of chains is determined to ensure that the model properties are representative of the behaviour of PE under rapid decompression. It has been confirmed that the selection of 20 chains, each containing 250 monomers, is sufficient to capture the mechanical behaviour of amorphous PE while balancing computational efficiency and maintaining accuracy [32].

After model construction, molecular interactions within the PE system are defined using the consistent valence forcefield (CVFF), which has been commonly used in previous simulation studies of polymer systems [33–41]. Specifically, bonded interactions include bond stretching, angle bending, dihedral torsion, and improper out-of-plane interactions between atoms [42]. For non-bonded interactions, a cut-off distance of 1 nm is utilized to compute van der Waals (vdW) and short-range Coulomb interactions, as these interactions are negligible beyond this distance [42]. Meanwhile, the particle-particle particle-mesh (PPPM) solver is employed to calculate long-range Coulomb interactions [42]. A time step of 1 femtosecond (fs) is used for these dynamic simulations.

In this study, MD simulations are conducted using the open-source code Large-scale Atomic/Molecular Massively Parallel Simulator (LAMMPS) [43]. During the MD simulation, the PE system is first subjected to an equilibration process to reach a stable state. The equilibration is performed in the isobaric-isothermal ensemble (NPT) at 250 K and 0 atm for 8 ns to ensure that the system's temperature, mean squared displacement (MSD), density, and total energy stabilized at constant levels [32]. The Nose-Hoover thermostat is used to control the temperature during the equilibration. As shown in Fig. 2, during the final 2 ns of the 8-ns NPT equilibration, the temperature, MSD, density, and total energy of the PE system stabilize at constant values, which indicates that the molecular model has reached equilibrium. The accuracy of this molecular model was validated in our recent study [30], where the predicted glass transition temperature (T_g = ~256 K), diffusion coefficient, and mechanical properties were in good agreement with simulation and experimental data.

2.2. Simulation details

Due to the pressure and time dependence of hydrogen molecule permeation and diffusion processes, which are challenging to simulate accurately within the spatial and temporal constraints of MD simulations, the permeation of hydrogen molecules into the polymer is not considered. Instead, the PE model is constructed containing specific concentrations of hydrogen molecules. To ensure the correct number of hydrogen molecules is present in the system for a realistic simulation, it is necessary to determine the solubility of hydrogen in the polymer. Accordingly, GCMC simulations are used to calculate the solubility and determine the appropriate number of hydrogen molecules in the PE system at various temperatures and pressures of interest. Briefly, the PE system is placed in contact with a virtual reservoir of hydrogen molecules at a given temperature and chemical potential, allowing for GCMC exchanges (i.e. insertion or deletion of hydrogen molecules). Each GCMC attempt is based on chemical potential energy considerations, which involves either inserting a hydrogen molecule at a random location in the simulation cell or deleting an existing hydrogen molecule, depending on the calculated energy change and acceptance criteria [44]. Due to variation in the number of hydrogen molecules in the system during the simulation, two identical Nose/Hoover thermostats are applied separately to both the PE and hydrogen, with each component being controlled individually. Prior to the GCMC simulation, the PE system is equilibrated for 2 ns at the corresponding temperature and pressure; the simulation then runs for an additional 2 ns, with 200

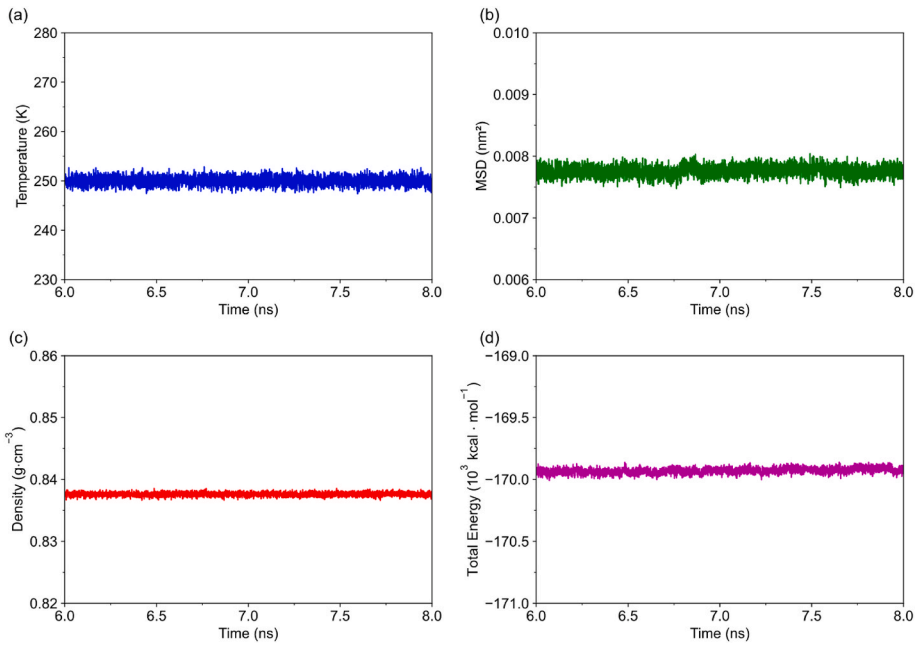


Fig. 2. (a) Temperature, (b) mean squared displacement (MSD), (c) density, (d) total energy of the PE system recorded during the final 2 ns of the equilibration process. The oscillation of these quantities around a steady average indicates that the equilibrium state is achieved.

GCMC exchanges attempted every 100 timesteps. The average number of hydrogen molecules over the last 1.5 ns of the GCMC simulation is used for the solubility calculation because the number of hydrogen molecules is stable during this period. The solubility is computed as the ratio of the mass of hydrogen molecules to the mass of the PE, as shown in the following equation:

$$S = \frac{m_{H_2}}{m_{PE}} \times 10^6 \text{ (ppm)} \quad (1)$$

where S represents the solubility in parts per million (ppm), m_{H_2} is the mass of hydrogen molecules, m_{PE} is the mass of the PE system, and 10^6 is a scaling factor to convert the ratio into ppm.

After determining the number of hydrogen molecules within the PE system under different conditions using GCMC, the MD simulation is equilibrated at an initially high pressure (ranging from 100 atm to 1000 atm, in intervals of 100 atm) for 2 ns, followed by decompression to 1 atm over 2 ns, and then equilibrated at 1 atm for a further 1 ns. The initial pressure range of 100–1000 atm is selected to cover a broad spectrum of potential operating conditions, as onboard storage for fuel cell vehicles are being designed to handle pressures up to 700 atm, and hydrogen fuel stations could operate at pressures reaching 1000 atm [9]. During the equilibration and decompression process, snapshots of the PE system are recorded at a time interval of 1 ps.

The fractional free volume (FFV) represents the proportion of unoccupied space between PE chains within the molecular structure. This free volume, which can potentially accommodate gas molecules, is analysed using OVITO, a visualization and analysis tool [45], with the alpha-shape method applied. In this study, the radius of the virtual spherical probe is set to 0.3 nm [10] corresponding to the equilibrium distance between hydrogen molecules as determined by prior research [46]. It is assumed that a minimum radius of 0.3 nm is required for the free volume to accommodate at least one hydrogen molecule. This is able to map accessible and inaccessible regions within the molecular structure by determining areas the probe can occupy without touching atomic sites. This enables the measurement of filled and empty space volumes and helps evaluate the porosity of the system. In the free volume analysis, only the polymer matrix is considered, which means hydrogen molecules are excluded from the free volume calculation. After initial equilibration, the system undergoes an instantaneous reduction to atmospheric pressure (1 atm) without any hydrogen molecules leaving the system i.e. diffusion of H_2 out of the polymer is neglected on this time scale.

This pressure change induces a volume expansion. Studying relative volume changes provides essential data for understanding how PE behaves under high-pressure hydrogen storage conditions. The relative change in total volume of the polymer is calculated using the following equation:

$$\text{Relative change in volume} = \left(V_f - V_i\right) / V_i \quad (2)$$

where V_f represents the time-averaged volume after decompression, and V_i represents the time-averaged volume before decompression.

To evaluate cavitation risk, the FFV before and after decompression is analysed. The change in FFV (i.e. ΔFFV) serves as an indicator of the susceptibility to cavitation. This approach is based on the premise that an increase in free volume creates localized cavities, which act as nucleation sites for cavitation. By quantifying ΔFFV, it is possible to assess the extent to which decompression induces structural instability within the polymer matrix, a critical factor in the initiation and propagation of cavitation [10].

Building on the established equilibration and decompression procedures as described above, the rapid decompression response of the PE system containing 155 hydrogen molecules is analysed in additional detail under conditions of room temperature (300 K) and an initial pressure of 700 atm; this is the upper range of working pressure for on board H_2 storage, making it a representative condition for practical applications. The number of hydrogen molecules (155) was derived from the solubility data obtained through GCMC simulations at 700 atm and 300 K. This analysis includes the evolution of free volume and different types of energy (i.e. non-bonded, bond, angle, dihedral, and total energy) during decompression and the radial distribution function of hydrogen molecules, both before and after decompression.

Subsequently, the impact of various factors on the FFV before and after decompression is examined, including initial pressure, temperature, and stress. These parameters are investigated because they directly affect key aspects of the PE behaviour, such as hydrogen solubility and diffusivity, the evolution of free volume, mechanical stability, and the cavitation risk during rapid decompression. Specifically, initial pressure

plays a pivotal role in determining both the hydrogen solubility within the polymer matrix and the mechanical response during decompression, which are key factors in assessing potential cavitation risks. In this study, an initial pressure range of 100–1000 atm is selected to comprehensively evaluate the effects of initial pressure on cavitation risk and material performance. Temperature also significantly affects the performance of on-board hydrogen storage tanks, which fluctuates due to hydrogen charging/discharging cycles and variations in ambient temperature. Since polymer properties are highly temperature-sensitive, it is crucial to evaluate how temperature impacts the decompression response of the polymer liner. The operational temperature range of hydrogen storage tanks typically spans from 233 K (−40 °C) to 358 K (85 °C) [9]. Therefore, this study simulates the rapid decompression behaviour of PE at six different temperatures ranging from 225 K to 350 K, with intervals of 25 K. Although the outer carbon fibre composite layer of high-pressure hydrogen storage tanks primarily withstands internal pressure, the polymer liner also deforms under this pressure, inevitably experiencing tensile stress. This occurs because, while the liner is compressed in the thickness direction due to the constraint imposed by the composite layer, it is also subjected to tensile stress in the circumferential direction as it expands to maintain the internal pressure of the tank. Evaluating the effect of stress on the polymer liner is important for understanding its mechanical stability during pressure changes. Based on previous MD simulation studies, the yield strength of PE exceeds 50 MPa [30]. Therefore, this study selects a tensile stress range of 0–50 MPa, with intervals of 10 MPa, to investigate the effect of stress on the rapid decompression behaviour of PE.

In studies of decompression damage in elastomers, it has been observed that the severity of damage increases with a higher decompression rate [48–50]. The decompression rate represents the amount of external high-pressure gas released per unit of time, typically measured in MPa•min^{-1} in experiments [11,47]. This rate determines the gas concentration gradient in polymers after decompression, which affects the stress values and stress distribution within the polymers [11]. Experimentally, transitions from pressurized to atmospheric conditions generally occur over a period ranging from minutes to hours [29]. The long durations used in experiments are difficult to achieve on the MD scale due to the extremely large number of time steps. Consequently, simulations are conducted for different decompression durations ranging from 1 to 30 ns, which is feasible with the computational resources available; this represents a worst-case scenario for rapid decompression damage, because the H_2 does not have time to diffuse from the polymer, thus it remains trapped, generating free volume. The increase in FFV on decompression is shown in Fig. 3. It is found that the decompression duration on the timescale of MD simulations has a minimal effect on the change in free volume. Therefore, considering the computational cost, the decompression duration is set to 2 ns.

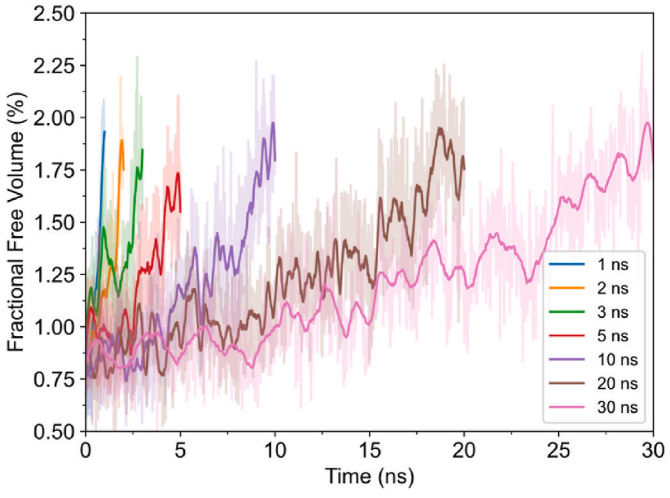


Fig. 3. FFV changes within the PE system under different decompression durations (initial pressure: 700 atm, temperature: 300 K). Solid lines represent a moving average with a window size of 50 ps?

3. Results and discussion

In this section, the solubility of hydrogen molecules in PE is first calculated. Afterwards, the molecular behaviours of PE during rapid decompression are presented and analysed, which include the evolution of FFV, the changes in free volume pore size, the radial distribution functions of hydrogen molecules, and the evolution of energy. Furthermore, the effects of initial pressure, temperature, and stress on relative volume change and FFV are discussed.

3.1. Hydrogen solubility in PE

The solubility of hydrogen molecules in amorphous PE derived from GCMC simulations at various temperatures and pressures is presented in Fig. 4. Table 1 compares the solubility of hydrogen molecules in PE at 700 atm and 300 K with a previous computational study, and with an experimental measurement for semicrystalline PE, with the H_2 in solution assigned entirely to the amorphous fraction. The solubility obtained in this study is 2245 ppm, which is very close to the previously obtained value of 2200 ppm [18], but higher than the experimental measurement of 1768 ppm [51]. This may be explained by the presence of the crystallites in suppressing solubility in the amorphous fraction below that predicted by the thermodynamic equilibrium [19]. As a result, the experimentally measured solubility is generally lower than that predicted by fully amorphous MD models.

The pressure effect on hydrogen solubility in amorphous PE differs below and above the T_g of 256 K. Fig. 4 shows that, at temperatures of 225 and 250 K, i.e. below the T_g, the solubility of hydrogen in the amorphous PE follows a typical Langmuir-type sorption behaviour (see Fig. 5), where solubility increases with pressure and then plateaus. Specifically, as pressure increases initially, gas molecules occupy the available free volume within the polymer, leading to an increase in solubility. Once the pressure reaches a certain threshold, the available free volume becomes saturated, and thus the solubility stops increasing

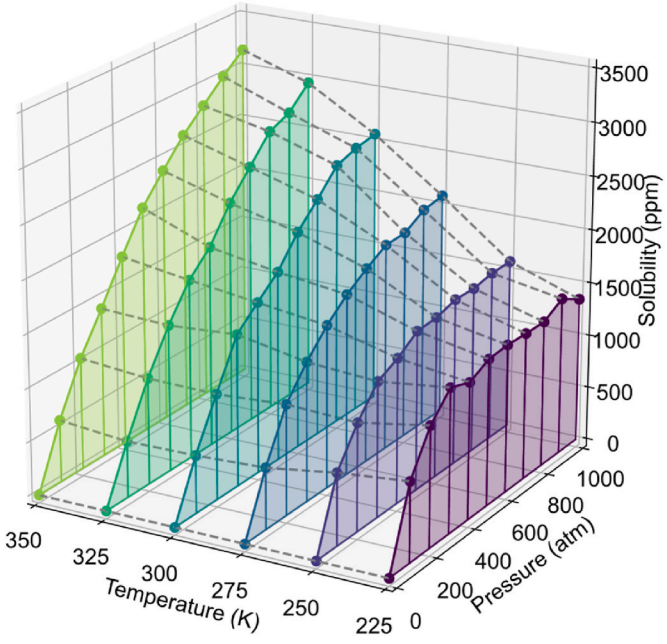


Fig. 4. Solubility of hydrogen molecules in amorphous PE as a function of temperature and pressure.

Table 1
Hydrogen solubility in PE under 700 atm pressure and 300 K.

Study	Method	Solubility (ppm)	Crystallinity (%)	Solubility in Amorphous Region (ppm)
This study	Simulation	2245	0	2245
Zhao et al. [18]	Simulation	2200	0	2200
Fujiwara et al. [51]	Experimental	831	53	1768

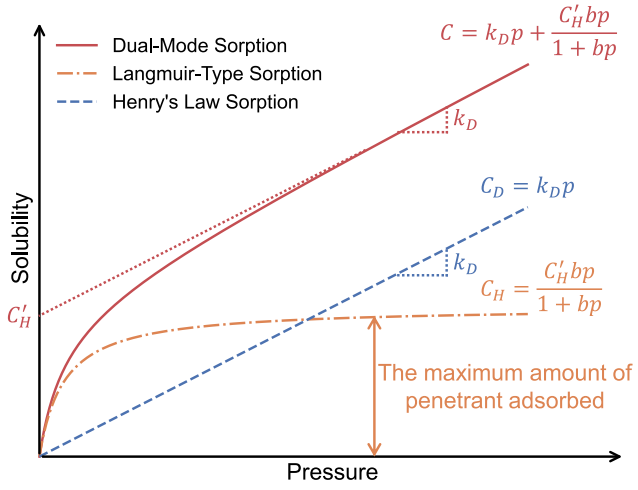


Fig. 5. Schematic representation of dual-mode sorption.

further. It is noted that at temperatures lower than T_g, the polymer is in a glassy state where molecular chain mobility is restricted, and the number of accessible sorption sites is limited. As the temperature increases, especially above T_g, the polymer chains gain more mobility, increasing the free volume within the amorphous regions. This allows more gas molecules to dissolve in the polymer, leading to a continuous rise in solubility with increasing pressure, albeit with a decreasing gradient. This behaviour is characteristic of dual-mode sorption [52], which is a combination of Henry's law sorption and Langmuir-type sorption. Specifically, Henry's law describes the linear increase in gas solubility with pressure, whereas Langmuir-type sorption accounts for the saturation of gas molecules in the finite free volume of the polymer. Thus, at low temperatures below T_g, the solubility eventually levels off, exhibiting the saturation characteristic of Langmuir-type sorption. At higher temperatures above T_g, the solubility continues to rise with increasing pressure, following the dual-mode sorption model. This reflects the complex interplay of gas adsorption mechanisms within the polymer under varying temperature and pressure.

The dual-mode sorption model in Fig. 5 is used to fit the solubility data as a function of pressure for various isotherms. The fitted parameters k_D, C_H, and b are summarized in Table 2. These parameters

Table 2
Fitted parameters of the dual mode sorption model in Fig. 5 at different temperatures.

Temperature (K)	k_D	C_H	b	R^2
225	4.1770×10^{-21}	1590.88	0.010140	0.9784
250	4.7167×10^{-15}	1920.93	0.005701	0.9952
275	1.1707×10^{-2}	2884.28	0.002728	0.9983
300	1.0295×10^{-2}	4394.68	0.001462	0.9971
325	4.2740×10^{-1}	4585.98	0.001221	0.9990
350	4.0050×10^{-1}	5177.42	0.001155	0.9995

quantitatively capture the transition from Langmuir-type sorption at low temperatures to dual-mode sorption at higher temperatures, reflecting the changing contributions of Henry's law and Langmuir-type sorption as the polymer transitions from a glassy to a rubbery state. Specifically, the increase in C_H and the decrease in b with temperature indicate a larger free volume and weaker adsorption affinity, respectively, while the small values of k_D highlight the limited contribution of Henry's law sorption at lower temperatures. In summary, below T_g, solubility follows Langmuir-type sorption with saturation at higher pressures, while above T_g, increased chain mobility and free volume lead to dual-mode sorption with solubility increasing continuously with pressure.

The effect of temperature on the solubility of hydrogen in amorphous PE differs between high- and low-pressure regimes. At pressures greater than 300 atm, the solubility of hydrogen increases significantly with increasing temperature. Conversely, at pressures below 300 atm, the solubility remains nearly constant across different temperatures, with variations from the average within 13%. Generally, the solubility of gases decreases as the temperature increases, as higher temperatures provide more energy for gas molecules to escape from the polymer matrix. However, in the case of gases with very low critical temperatures, such as hydrogen and nitrogen, the opposite trend is observed, known as reverse solubility [53,54]. This behaviour can also be explained by the competing effects of the negative change in the entropy of H_2 during condensation and the positive entropy change on mixing the condensed H_2 with the polymer. An increase in solubility with increasing temperature occurs when the positive entropy change from mixing condensed H_2 with the polymer dominates over the negative entropy change from condensation. The insensitivity of H_2 solubility in PE at lower temperatures suggests that these entropic effects cancel out. At higher pressures, the entropy of gaseous hydrogen is reduced, whilst the entropy of the condensed hydrogen remains approximately constant, thus the entropy change of condensation becomes less negative. Consequently, the positive entropy change on mixing dominates at higher pressures, resulting in the observed increase in solubility with temperature.

Thus, the trends in the solubility of H_2 in amorphous PE with temperature and pressure are complex and cannot be easily generalized. The behaviour observed at low pressures or temperatures cannot be directly extrapolated to high pressures or temperatures due to the non-linear interplay of thermodynamic factors such as entropy and free volume. To fully understand the behaviour of PE under a wide range of pressure and temperature conditions, a large number of time consuming and costly experiments would be required. This study highlights the power of MD simulations and numerical modelling as effective tools for providing a comprehensive understanding of the response of PE in hydrogen environments, enabling insights that are otherwise difficult to determine experimentally.

3.2. Decompression response of PE

This section provides a detailed analysis of the decompression response of the amorphous PE containing 155 hydrogen molecules at 300 K, with an initial pressure of 700 atm and a final pressure of 1 atm. The evolution of free volume in the PE system during the decompression process is shown in Fig. 6. Under the initial high-pressure condition (700 atm), the FFV is relatively low, and the size of individual pores remains small. As the pressure decreases, the FFV more than doubles from 0.88% to 2.01%, with the quantity of cavities increasing from 42 to 80, and the average size of individual pores increasing from 0.06 nm^3 to 0.07 nm^3. We hypothesise that the expansion of free volume creates favourable conditions for the initiation of cavitation within the polymer matrix i.e. the enlarged free volume at the nanoscale, caused by the pressure drop, expands and agglomerates into larger cavities. In this case, the microscopic increase in free volume and pore size observed in this theoretical work would be directly linked to the occurrence of cavitation and foaming in the polymer during rapid decompression.

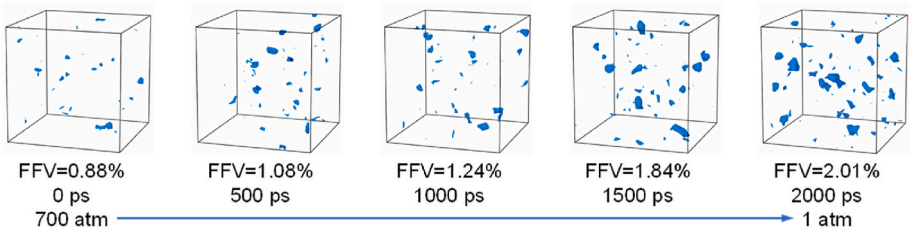


Fig. 6. Free volume evolution of PE systems with 155 hydrogen molecules after a decompression from 700 atm to 1 atm at 300 K, recorded at 0, 500, 1000, 1500, and 2000 ps.

To further quantify the evolution of free volume in the PE system during decompression, pore sizes are measured at 10 ps intervals. Fig. 7 (a) is a scatter plot showing individual pore sizes as pressure decreases from 700 to 1 atm. Each data point represents the size of a free volume pore at a specific frame, and red points represents the maximum pore size observed in each frame. The majority of pore sizes are below 0.2 nm^3, consistent with previous MD simulations of EPDM, which reported similar pore size distributions [29]. It can be seen that the maximum pore size increases as pressure drops; by the end of the decompression process, the maximum pore size approaches approximately 0.7 nm^3. Fig. 7(b) compares the pore size distribution curves before and after decompression, revealing a remarkable increase in both the number and size of pores, highlighting the considerable growth in free volume within the polymer matrix. Interestingly, new regions of free volume are generated, where none previously existed. This observation suggests that the generation of free volume during decompression is not limited to pre-existing pores in the polymer matrix. Instead, decompression can induce the formation of new regions of free volume. This phenomenon is attributed to the redistribution and relative motion of polymer chains during the decompression process.

Investigating the distribution of hydrogen molecules is crucial to understand how decompression impacts hydrogen clustering and dispersion within the polymer matrix, which directly affects the potential for localized accumulation and cavitation risks. The radial distribution function $g(r)$ quantifies the probability of finding a pair of particles separated by a distance r. In this study, $g(r)$ is used to analyse the spatial distribution of hydrogen molecules before and after decompression. Given the relatively low concentration of hydrogen molecules in the PE system, the resulting radial distribution function curves showed noticeable fluctuations. To improve accuracy, the curves are time-averaged over a 1 ns interval both before and after decompression. The radial distribution function for the PE system containing 155 hydrogen molecules is shown in Fig. 8. Additionally, the radial distribution function for a pure hydrogen gas system, calculated through MD simulations, is provided for comparison. The peak in the $g(r)$ curve occurs at a distance of approximately 0.3 nm, which corresponds to the typical intermolecular distance at which hydrogen molecules exhibit local clustering within the amorphous PE matrix [29]. The height of the peak of hydrogen molecules in PE is significantly higher than that of

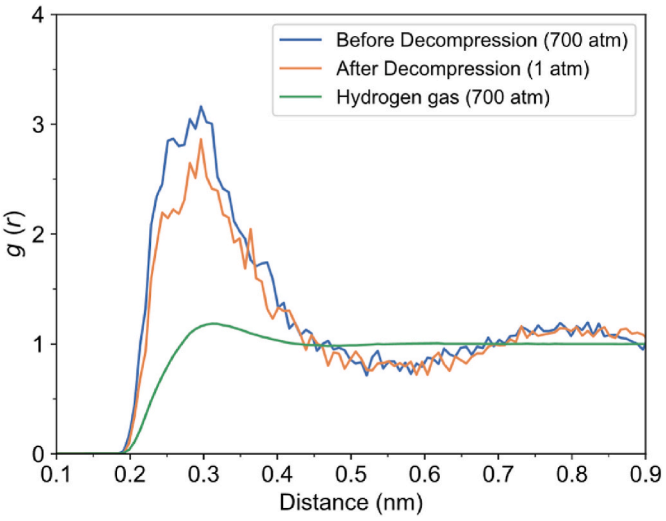


Fig. 8. Radial distribution functions for hydrogen molecules before and after decompression (system containing 155 H_2 molecules, 300 K).

gaseous hydrogen molecules, which indicates that the hydrogen molecules dissolved in the polymer exist in a condensed state [29]. After decompression, there is a slight reduction in the height of the peak, suggesting a marginal decrease in hydrogen clustering after decompression. This reduction results primarily from the increased volume of the system as pressure is released, allowing the hydrogen molecules to become more dispersed within the polymer matrix [29]. The minor changes in the radial distribution functions after decompression reveal that while decompression leads to an expansion in free volume, the spatial arrangement of hydrogen molecules within the PE system is not drastically altered. The observed reduction in clustering after decompression indicates a diminished probability of hydrogen molecules forming local clusters.

Understanding how internal energy evolves during decompression helps identify specific molecular behaviours, such as chain mobility and conformational shifts, that contribute to the response of material under

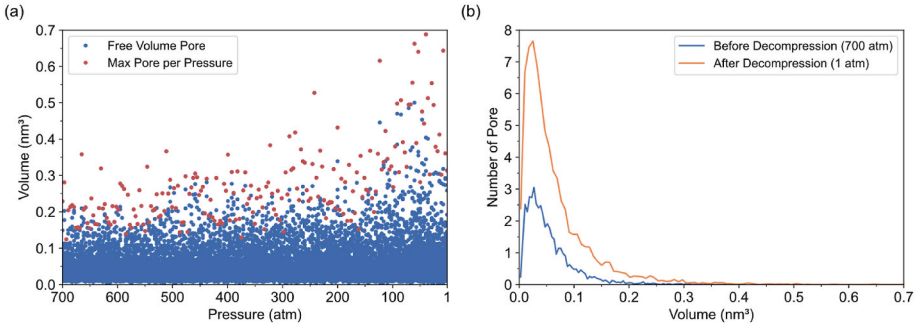


Fig. 7. (a) Scatter plot of free volume pore size evolution during decompression process, (b) distribution of free volume pore size before and after decompression.

extreme conditions. The energy changes in the PE system during rapid decompression are depicted in Fig. 9. The energies associated with bond stretching (E_{bond}) and bond angles (E_{angle}) show minimal fluctuations, indicating that the intramolecular geometry of the PE molecules remains stable during the decompression process. A slight reduction in dihedral energy ($E_{dihedral}$) is observed during decompression, which suggests minor conformational adjustments in the dihedral angles. Specifically, some molecules undergo a transition from higher-energy gauche conformations to more stable trans conformations, as shown in Fig. 10. This transition is driven by the volumetric expansion, which allows polymer chains to extend and straighten. The increased chain mobility, resulting from the reduction in intermolecular forces, permits these internal rearrangements, enabling the polymer to adopt more stable, lower-energy conformations. The total energy (E_{total}) of the system shows an overall increase during decompression, primarily due to an increase in non-bonded interaction energies ($E_{non\text{-}bonded}$). As the system expands, the distances between molecules increase, leading to a rise in vdW forces and short-range Coulombic interactions. While decompression weakens intermolecular attractions, the expanded volume increases non-bonded interaction energy, thus contributing to the overall increase in system energy.

3.3. Effect of various initial conditions on relative volume change & FFV

3.3.1. Effect of initial pressure

Based on the solubility results presented and discussed in Section 3.1, the number of hydrogen molecules present in the PE system is determined at a constant temperature of 300 K under varying initial pressures, ranging from 100 atm to 1000 atm in increments of 100 atm. NPT dynamics is then applied to the PE system to rapidly decompress from the initial pressure to 1 atm over a simulation period of 2 ns. The changes in both bulk volume and FFV before and after decompression are compared in Fig. 11. As shown in Fig. 11(a), the relative volume change increases approximately linearly with the initial pressure. When the initial pressure is set to 100 atm, the relative volume change is 0.48%, whereas at an initial pressure of 1000 atm, the relative volume change reaches 4.80%. Thus, higher initial pressures lead to more significant volume expansion during decompression.

Following the examination of bulk volume changes, the risk of cavitation is evaluated through changes in free volume. As illustrated in Fig. 11(b), the initial FFV before decompression decreases slightly with initial pressure, owing to mechanical compression of the polymer. The amount of hydrogen molecules present in the system increases with higher initial pressures, creating more free volume. However, higher initial pressures also compress the polymer chains, which reduces the free volume. The compressive effect of the pressure dominates, resulting in a net decrease in the FFV before decompression as initial pressure increases. After decompression, the FFV is higher in PE systems that initially have higher pressures. This is because, after decompression to atmospheric pressure, the PE systems with higher initial pressures contain more hydrogen molecules, which introduce additional free volume into the polymer matrix. To assess the risk of cavitation, the difference in FFV before and after decompression is considered; the increase in free volume provides potential sites for gas localization, which could act as precursors to cavitation-induced failure. The difference in FFV increases with higher initial pressures, indicating that greater initial pressures lead to a higher risk of cavitation, which is observed in practice [24]. This is attributed to two main factors: firstly, the higher initial pressure causes more compression, leading to greater expansion of volume upon decompression; and secondly, the increased number of hydrogen molecules creates more free volume, which becomes more pronounced after decompression.

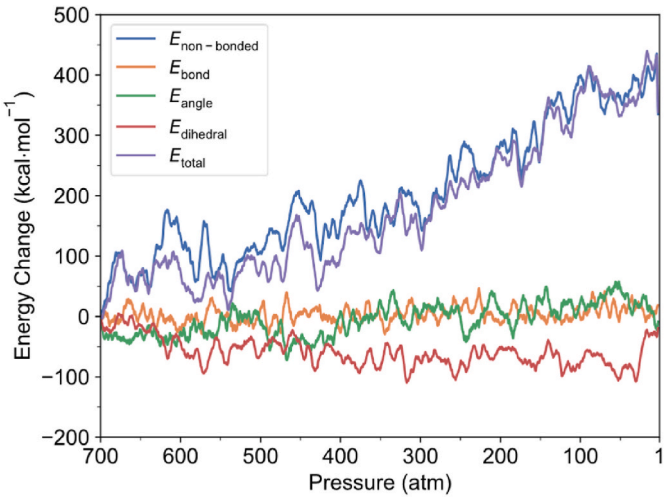


Fig. 9. Energy changes of the PE system during rapid decompression.

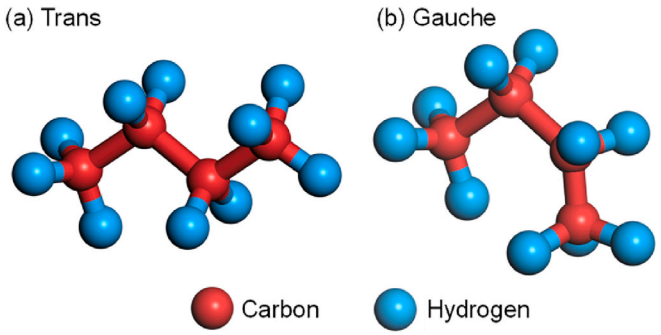


Fig. 10. Schematic diagram of trans and gauche conformations.

3.3.2. Effect of temperature

The initial pressure of the PE systems is set to 700 atm, with the number of hydrogen molecules determined based on the solubility data from Section 3.1. As shown in Fig. 12, the relative volume change of the PE system increases approximately linearly with temperature. At higher temperatures, the polymer chains exhibit greater mobility, allowing them to adjust and move further apart, resulting in an increase in the overall system volume. The FFV of the PE system also increases with increasing temperatures, both before and after decompression. Notably, at temperatures lower than the T_g of 256 K, the FFV remains relatively constant, indicating minimal changes in free volume with temperature in the glassy state; however, above T_g, the FFV increases significantly with increasing temperature. Below T_g, the polymer is in a glassy state with restricted chain mobility, limiting changes in free volume. The inherent cavities within the polymer remain constant, resulting in a stable FFV despite temperature variations. As temperature increases above T_g, the increased kinetic energy of the polymer chains results in more vigorous molecular motion, which enlarges the average spacing between chains and increases the free volume within the polymer matrix. Meanwhile, the solubility of hydrogen in PE increases with temperature, as reported in Section 3.1. At higher temperatures, the polymer matrix accommodates a larger number of hydrogen molecules. This elevated hydrogen content further contributes to the increase in free volume, as the dissolved hydrogen molecules create additional spaces within the polymer structure. The combined effects of enhanced polymer chain mobility and higher hydrogen solubility result in a more significant expansion of free volume at elevated temperatures. The difference in free volume before and after decompression also grows with increasing temperature above T_g, suggesting that the risk of cavitation during rapid decompression becomes greater at higher temperatures; again, this same trend is observed in practice [20–23]. As the temperature increases, the enhanced mobility of polymer chains creates more potential sites for gas localization. These caivities grow and merge,

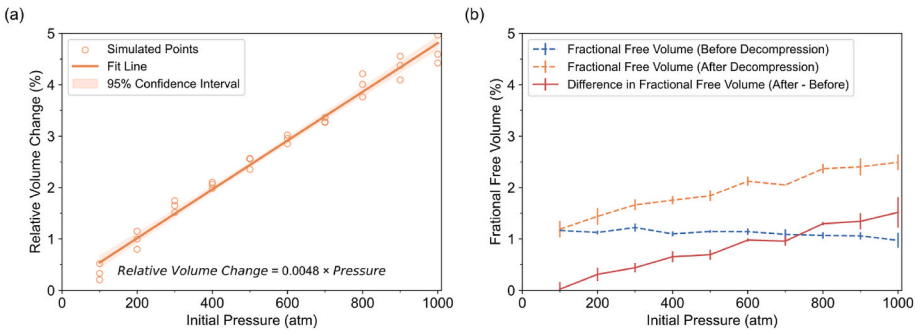


Fig. 11. Effect of initial pressure on the (a) relative volume change and (b) FFV in the PE system before and after decompression. (The hydrogen content of the PE in each simulation uses the results of the solubility simulations at 300 K and the corresponding initial pressure).

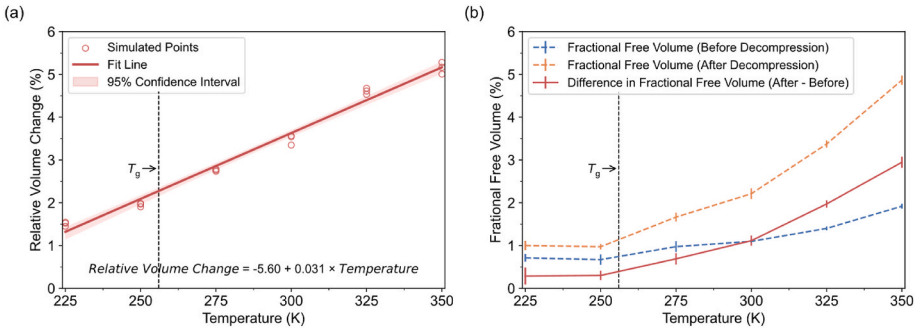


Fig. 12. Effect of temperature on the (a) relative volume change and (b) FFV in the PE system before and after decompression (initial pressure: 700 atm).

leading to cavitation-induced failure.

3.3.3. *Effect of tensile stress*

Fig. 13 (a) shows that when the liner is under tensile stress, the overall relative volume change upon decompression initially decreases significantly as the tensile stress increases up to 10 MPa. This behaviour can be attributed to the elevated stress enhancing the orientation of polymer chains, allowing the material to better resist volumetric expansion during decompression. This occurs because stress increases the orientation of polymer chains, enabling the material to better resist volumetric expansion during decompression [30]. However, as the tensile stress increases beyond 10 MPa, the relative volume change stabilizes and shows no significant variation, remaining approximately constant. Interestingly, the FFV in PE increases with increasing tensile stress, as illustrated in Fig. 13(b). This does not contradict the observed decrease in relative volume change under tensile stress, as the total volume increases with increasing tensile stress, allowing more free volume to form within the polymer matrix. This effect, where tensile stress increases the free volume in the PE material, has also been demonstrated in our previous studies [30]. Notably, it can be seen in Fig. 13(b) that the difference in free volume before and after decompression also rises with increasing tensile stress, suggesting that it exacerbates cavitation during rapid decompression. This occurs because applied stress stretches and reorients polymer chains, increasing interstitial spaces and reducing chain entanglement [30]. Upon decompression, these stress-induced spaces expand more readily, allowing cavities to form. Consequently, higher tensile stress enhances free volume expansion, raising the risk of cavitation. Once again this finding from our MD simulations is consistent with that observed experimentally in PVDF, whereby applied tension during hydrogen decompression was found to promote cavitation; it was suggested that this resulted from increasing cavity nucleation and coalescence, ultimately increasing the surface coverage of cavities in the polymer material [26].

3.4. *Summary of the effect of high-pressure hydrogen decompression in PE*

The primary findings of this study reveal changes in hydrogen

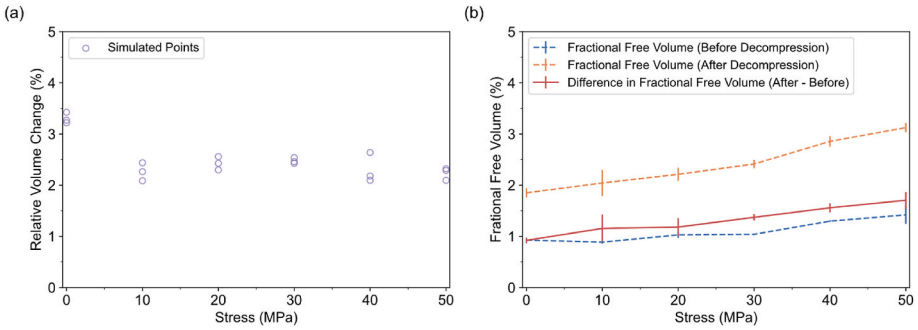


Fig. 13. Effect of tensile stress on the (a) relative volume change on decompression and (b) FFV in the PE system before and after decompression (temperature: 300 K, initial pressure: 700 atm).

solubility, and variations in FFV of the amorphous PE at different pressures and temperatures, offering insights into the molecular-level effects of rapid decompression on PE. Specifically, rapid decompression causes volumetric expansion of PE, which increases the intermolecular distances between polymer chains, leading to an increase in the internal free volume. The quantity of hydrogen molecules dissolved in the PE (i.e. its solubility) plays a critical role in this process. As more hydrogen molecules occupy the spaces between polymer chains, they create additional free volume within the polymer matrix. Our MD study further supplements and quantifies the influence of initial pressure on the rapid decompression response of PE at the nanoscale. Specifically, higher initial pressures lead to a more significant increase in free volume, which can primarily be attributed to the increased hydrogen solubility in PE prior to decompression. Macroscopic mechanical properties of the polymer are highly sensitive to temperature, thus an increase in temperature often results in a decline in mechanical performance, which subsequently raises the cavitation risk [55]. Our study further reveals that, at the nanoscale, an increase in temperature leads to a significant rise in free volume in the PE, and greater free volume generation on decompression; increasing tensile stress has a similar effect. These trends in free volume generation with temperature, pressure and tensile stress from our MD simulations are consistent with those observed experimentally for the risk of cavitation damage. This lends weight to the hypothesis that free volume generation represents the onset of the formation of cavities on the nanoscale, previously observed by TEM [26], ultimately resulting in cavitation failure.

Based on the analysis presented in this study, the following strategies are recommended to mitigate cavitation-induced failure in the polymer liners of hydrogen storage tanks. One key approach is managing hydrogen solubility by designing the polymer to limit hydrogen uptake or controlling the hydrogen concentration during use, which helps minimize the contribution of dissolved hydrogen to free volume expansion during decompression. Reducing the initial pressure during the decompression process is also crucial, as the analysis shows that the FFV increases significantly when the initial pressure exceeds 700 atm. Temperature control is another important factor, as high temperatures promote an increase in free volume within the polymer, facilitating cavity formation. It is found that temperatures above 300 K result in a significant increase in FFV generation on decompression, making it advisable to keep the temperature below this threshold. Additionally, elevated temperatures reduce the mechanical strength of the polymer [30], further raising the risk of failure during decompression. Minimizing the tesnile stress applied on the polymer liner is also recommended to mitigate cavitation risks. Lower stress levels help prevent excessive deformation and limit the formation of large free volumes.

One of the primary limitations of this study is the constraint of MD simulations, particularly the limited time and spatial scales that can be practically simulated. Secondly, the study focuses solely on the amorphous regions of PE, excluding any crystalline content. Since real-world PE typically contains both amorphous and crystalline phases, the exclusion of crystalline regions may limit how well these findings apply to semicrystalline materials. Meanwhile, the MD model used in this study does not include specific damage criteria, which limits the ability to predict the onset of material failure.

To address the limitations outlined above, future studies can consider employing coarse-grained MD simulations to incorporate crystalline regions, building on the atomistic simulations presented in this study. This approach helps to develop a more comprehensive understanding of semicrystalline PE behaviour under decompression. Broader studies involving other polymers and composite materials would further enhance the generalizability and applicability of these findings to a wider range of hydrogen storage solutions. Future work could establish relevant damage criteria, such as considering damage initiation when individual free volume pore sizes reach a critical threshold, to better assess material degradation and failure mechanisms.

4. Conclusions

This study investigates the solubility of hydrogen and the decompression response of amorphous PE under high-pressure hydrogen environments using atomistic MD simulations. At the molecular level, rapid decompression involves volumetric expansion of the polymer matrix, leading to a significant increase in internal free volume. This process is facilitated by hydrogen molecules, which enhance free volume generation through their interaction with the polymer chains. These molecular-scale mechanisms provide a fundamental understanding of how hydrogen solubility, free volume changes, and cavitation risk evolve under varying pressure, temperature, and tensile stress. The key conclusions are:

- Solubility of hydrogen: The solubility of hydrogen in amorphous PE exhibits distinct behaviours depending on the temperature and pressure regimes. Below T_g, the polymer is in a glassy state, and solubility follows a Langmuir-type sorption model, where free volume is limited, and solubility eventually saturates with increasing pressure. Above T_g, solubility is governed by a dual-mode sorption model, combining Henry's law and Langmuir-type sorption. At low pressures below 300 atm, the effect of temperature on solubility is minimal. In contrast, at higher pressures, solubility increases with temperature. This highlights the critical influence of the state of the amorphous polymer (rubbery or glassy) and the interplay of temperature and pressure on hydrogen solubility.
- Energy changes during decompression: The analysis of internal energy reveals that non-bonded interactions between polymer chains dominate the energy changes during decompression, as the intermolecular distances increase. This increase in intermolecular distances reduces the cohesive forces within the polymer matrix, creating favourable conditions for free volume generation, leading to cavity formation and ultimately cavitation damage.
- Factors increasing cavitation risk: Higher initial pressures, hydrogen content, temperature, and applied tensile stress significantly amplify the increase in free volume on decompression, thereby elevating the cavitation risk.

This study provides critical insights into the solubility and decompression behaviour of amorphous PE under high-pressure hydrogen environments, at the molecular scale. The findings emphasize the importance of controlling external parameters such as temperature, pressure, and hydrogen content to reduce cavitation risk and enhance the durability of polymer liners in hydrogen storage applications.

CRediT authorship contribution statement

Guozhen Ding: Conceptualization, Formal analysis, Methodology, Software, Visualization, Writing – original draft. **Christopher J. Tighe:** Writing – review & editing. **Lik-ho Tam:** Methodology, Validation, Visualization, Writing – review & editing. **Chao Wu:** Conceptualization, Formal analysis, Methodology, Project administration, Resources, Supervision, Writing – original draft, Writing – review & editing.

Declaration of competing interest

The authors declare that they have no known competing financial interests or personal relationships that could have appeared to influence the work reported in this paper.

Acknowledgement

Guozhen Ding acknowledges financial support from the Imperial College President's PhD Scholarships. Chao Wu acknowledges the support by the UKRI Future Leaders Fellowship (MR/X034054/1). We additionally acknowledge computational resources and support

provided by the Research Computing Service and the Composites for Energy Infrastructure Group at Imperial College London. The last author thanks Jingheng (Hadan) Wu for his consistent support and inspiration.

References

[1] Meda US, Rajyaguru YV, Pandey A. Generation of green hydrogen using self-sustained regenerative fuel cells: opportunities and challenges. Int J Hydrogen Energy 2023;48:28289–314. https://doi.org/10.1016/j.ijhydene.2023.03.430.

[2] Rasul MG, Hazrat MA, Sattar MA, Jahirul MI, Shearer MJ. The future of hydrogen: challenges on production, storage and applications. Energy Convers Manag 2022; 272:116326. https://doi.org/10.1016/j.enconman.2022.116326.

[3] Olabi AG, bahri A saleh, Abdelghafar AA, Baroutaji A, Sayed ET, Alami AH, et al. Large-vscale hydrogen production and storage technologies: current status and future directions. Int J Hydrogen Energy 2021;46:23498–528. https://doi.org/10.1016/j.ijhydene.2020.10.110.

[4] Qureshi F, Yusuf M, Arham Khan M, Ibrahim H, Ekeoma BC, Kamyab H, et al. A State-of-The-Art Review on the Latest trends in Hydrogen production, storage, and transportation techniques. Fuel 2023;340:127574. https://doi.org/10.1016/j.fuel.2023.127574.

[5] Faye O, Szpunar J, Eduok U. A critical review on the current technologies for the generation, storage, and transportation of hydrogen. Int J Hydrogen Energy 2022; 47:13771–802. https://doi.org/10.1016/j.ijhydene.2022.02.112.

[6] Laureys A, Depraetere R, Cauwels M, Depover T, Hertelé S, Verbeken K. Use of existing steel pipeline infrastructure for gaseous hydrogen storage and transport: a review of factors affecting hydrogen induced degradation. J Nat Gas Sci Eng 2022; 101:104534. https://doi.org/10.1016/j.jngse.2022.104534.

[7] Zheng J, Liu X, Xu P, Liu P, Zhao Y, Yang J. Development of high pressure gaseous hydrogen storage technologies. Int J Hydrogen Energy 2012;37:1048–57. https://doi.org/10.1016/j.ijhydene.2011.02.125.

[8] Andersson J, Grönkvist S. Large-scale storage of hydrogen. Int J Hydrogen Energy 2019;44:11901–19. https://doi.org/10.1016/j.ijhydene.2019.03.063.

[9] Balasooriya W, Clute C, Schrittesser B, Pinter G. A review on applicability, limitations, and improvements of polymeric materials in high-pressure hydrogen gas atmospheres. Polym Rev 2022;62:175–209. https://doi.org/10.1080/15583724.2021.1897997.

[10] Zhao J, Wang X, Yang Q, Yin H, Zhao B, Zhang S, et al. Molecular dynamics simulation of H2 in amorphous polyethylene system: H2 diffusion in various PE matrices and bubbling during rapid depressurization. Int J Hydrogen Energy 2022; 47:39572–85. https://doi.org/10.1016/j.ijhydene.2022.09.124.

[11] Jin Z, Su Y, Lv H, Liu M, Li W, Zhang C. Review of decompression damage of the polymer liner of the type IV hydrogen storage tank. Polymers 2023;15:2258. https://doi.org/10.3390/polym15102258.

[12] Melnichuk M, Thiébaud F, Perreux D. Non-dimensional assessments to estimate decompression failure in polymers for hydrogen systems. Int J Hydrogen Energy 2020;45:6738–44. https://doi.org/10.1016/j.ijhydene.2019.12.107.

[13] Kulkarni SS, Choi KS, Menon N, Simmons K. A diffusion–deformation model with damage for polymer undergoing rapid decompression failure. J Mech Phys Solid 2023;178:105348. https://doi.org/10.1016/j.jmps.2023.105348.

[14] Zhou C, Liu X, Zheng Y, Hua Z. A comprehensive review of hydrogen-induced swelling in rubber composites. Compos Part B Eng 2024;275:111342. https://doi.org/10.1016/j.compositesb.2024.111342.

[15] Alkire JD, Mason JF. Effect of rapid decompression conditions on liner materials. OnePetro; 2000.

[16] Yersak TA, Baker DR, Yanagisawa Y, Slavik S, Immel R, Mack-Gardner A, et al. Predictive model for depressurization-induced blistering of type IV tank liners for hydrogen storage. Int J Hydrogen Energy 2017;42:28910–7. https://doi.org/10.1016/j.ijhydene.2017.10.024.

[17] Fujiwara H, Ono H, Ohyama K, Kasai M, Kaneko F, Nishimura S. Hydrogen permeation under high pressure conditions and the destruction of exposed polyethylene-property of polymeric materials for high-pressure hydrogen devices (2)-. Int J Hydrogen Energy 2021;46:11832–48. https://doi.org/10.1016/j.ijhydene.2020.12.223.

[18] Zhao J, Li X, Wang X, Zhang Q, Yang Q, Yin H, et al. Insights into the solubility of H2 in various polyethylene matrices at high pressure: a coarse-grained MC/MD study. Int J Hydrogen Energy 2023;48:19619–32. https://doi.org/10.1016/j.ijhydene.2023.02.026.

[19] Atiq O, Ricci E, Baschetti MG, De Angelis MG. Modelling solubility in semi-crystalline polymers: a critical comparative review. Fluid Phase Equilib 2022;556: 113412. https://doi.org/10.1016/j.fluid.2022.113412.

[20] Rueda F, Torres JP, Machado M, Frontini PM, Otegui JL. External pressure induced buckling collapse of high density polyethylene (HDPE) liners: FEM modeling and predictions. Thin-Walled Struct 2015;96:56–63. https://doi.org/10.1016/j.tws.2015.04.035.

[21] Rueda F, Marquez A, Otegui JL, Frontini PM. Buckling collapse of HDPE liners: experimental set-up and FEM simulations. Thin-Walled Struct 2016;109:103–12. https://doi.org/10.1016/j.tws.2016.09.011.

[22] Pépin J, Lainé E, Grandidier J-C, Benoit G, Mellier D, Weber M, et al. Replication of liner collapse phenomenon observed in hyperbaric type IV hydrogen storage vessel by explosive decompression experiments. Int J Hydrogen Energy 2018;43: 4671–80. https://doi.org/10.1016/j.ijhydene.2018.01.022.

[23] Pepin J, Lainé E, Grandidier J-C, Castagnet S, Blanc-vannet P, Papin P, et al. Determination of key parameters responsible for polymeric liner collapse in hyperbaric type IV hydrogen storage vessels. Int J Hydrogen Energy 2018;43: 16386–99. https://doi.org/10.1016/j.ijhydene.2018.06.177.

[24] Blanc-Vannet P, Papin P, Weber M, Renault P, Pepin J, Lainé E, et al. Sample scale testing method to prevent collapse of plastic liners in composite pressure vessels. Int J Hydrogen Energy 2019;44:8682–91. https://doi.org/10.1016/j.ijhydene.2018.10.031.

[25] Ono H, Fujiwara H, Onoue K, Nishimura S. Influence of repetitions of the high-pressure hydrogen gas exposure on the internal damage quantity of high-density polyethylene evaluated by transmitted light digital image. Int J Hydrogen Energy 2019;44:23303–19. https://doi.org/10.1016/j.ijhydene.2019.07.035.

[26] Gerland M, Boyer SAE, Castagnet S. Early stages of cavitation in a stretched and decompressed poly(vinylidene fluoride) exposed to diffusive hydrogen, observed by Transmission Electronic Microscopy at the nanoscale. Int J Hydrogen Energy 2016;41:1766–74. https://doi.org/10.1016/j.ijhydene.2015.11.015.

[27] Kulkarni SS, Choi KS, Kuang W, Menon N, Mills B, Soulami A, et al. Damage evolution in polymer due to exposure to high-pressure hydrogen gas. Int J Hydrogen Energy 2021;46:19001–22. https://doi.org/10.1016/j.ijhydene.2021.03.035.

[28] Li Y, Shin Y, Kuang W, Simmons KL. Phase field modeling of hydrogen release in nitrile-butadiene rubber composites after high-pressure hydrogen exposure. Int J Hydrogen Energy 2024;59:833–44. https://doi.org/10.1016/j.ijhydene.2024.02.017.

[29] Wilson MA, Frischknecht AL. High-pressure hydrogen decompression in sulfur crosslinked elastomers. Int J Hydrogen Energy 2022;47:15094–106. https://doi.org/10.1016/j.ijhydene.2022.03.015.

[30] Ding G, Tam L, Wu C. Molecular investigation on physical and tensile properties of polyethylene (PE) under high-pressure hydrogen environments. Int J Hydrogen Energy 2024;86:1036–50. https://doi.org/10.1016/j.ijhydene.2024.08.487.

[31] Wilson MA, Brownell M, Frischknecht AL. Atomistic materials modeling of high-pressure hydrogen interactions in ethylene propylene diene monomer (EPDM) rubber. Albuquerque, NM (United States): Sandia National Lab. (SNL-NM); 2022. https://doi.org/10.2172/1898282.

[32] Bowman AL, Mun S, Nouranian S, Huddleston BD, Gwaltney SR, Baskes MI, et al. Free volume and internal structural evolution during creep in model amorphous polyethylene by Molecular Dynamics simulations. Polymer 2019;170:85–100. https://doi.org/10.1016/j.polymer.2019.02.060.

[33] Wu C, Wu R, Tam L. Coarse-grained molecular simulation of the effects of carbon nanotube dispersion on the mechanics of semicrystalline polymer nanocomposites. Nanotechnology 2021;32:325705. https://doi.org/10.1088/1361-6528/abf458.

[34] Wu R, Wang XQ, Zhao D, Hou J, Wu C, Lau D, et al. Degradation of fiber/matrix interface under various environmental and loading conditions: insights from molecular simulations. Constr Build Mater 2023;390:131101. https://doi.org/10.1016/j.conbuildmat.2023.131101.

[35] Tam L, Lau D. Effect of structural voids on mesoscale mechanics of epoxy-based materials. Coupled Syst Mech 2016;5:355–69. https://doi.org/10.12989/csm.2016.5.4.355.

[36] Cai G, Zhang D, Hou J, Lau D, Qin R, Wang W, et al. Machine learning prediction models for investigating vibration properties of epoxy resin under moisture conditions. Int J Non-Linear Mech 2024;166:104857. https://doi.org/10.1016/j.ijnonlinmec.2024.104857.

[37] Tam L, Wu R, Hou J, Wu C. Molecular simulation investigations of property degradation in CFRP composite. Singapore: Springer Nature Singapore; 2024. https://doi.org/10.1007/978-981-97-3901-1.

[38] Wu C, Wu R, Tam L. The creep behavior of semicrystalline carbon nanotube/polypropylene nanocomposite: a coarse-grained molecular study. Polym Degrad Stabil 2022;196:109834. https://doi.org/10.1016/j.polymdegradstab.2022.109834.

[39] Wu C, Wu R, Xia W, Tam L. Understanding creep behavior of semicrystalline polymer via coarse-grained modeling. J Polym Sci, Part B: Polym Phys 2019;57: 1779–91. https://doi.org/10.1002/polb.24912.

[40] Tam L, Wu R, Minkeng MAN, Jiang J, Zhou A, Hao H, et al. Understanding creep behavior of carbon fiber/epoxy interface via molecular dynamics simulation. Mech Adv Mater Struct 2023;30:4052–64. https://doi.org/10.1080/15376494.2022.2088906.

[41] Wu C, Hou J, Liu H, Yang J, Lau D, Tam L. Understanding moisture effect on nonlinear vibrations of epoxy thin film via a multiscale simulation. J Sound Vib 2023;553:117649. https://doi.org/10.1016/j.jsv.2023.117649.

[42] Hockney RW, Eastwood JW. Computer simulation using particles. Boca Raton: CRC Press; 2021. https://doi.org/10.1201/9780367806934.

[43] Thompson AP, Aktulga HM, Berger R, Bolintineanu DS, Brown WM, Crozier PS, et al. Lammps - a flexible simulation tool for particle-based materials modeling at the atomic, meso, and continuum scales. Comput Phys Commun 2022;271:108171. https://doi.org/10.1016/j.cpc.2021.108171.

[44] Barraco M, Neyertz S, Benes NE, Brown D. Comparison of eight classical Lennard-Jones-based H_2 molecular models in the gas phase at temperatures and pressures relevant to hydrogen on-board storage tanks. J Phys Chem A 2023;127:6335–46. https://doi.org/10.1021/acs.jpca.3c03212.

[45] Stukowski A. Visualization and analysis of atomistic simulation data with OVITO–the Open Visualization Tool. Model Simulat Mater Sci Eng 2009;18: 015012. https://doi.org/10.1088/0965-0393/18/1/015012.

[46] Mason EA, Rice WE. The intermolecular potentials of helium and hydrogen. J Chem Phys 1954;22:522–35. https://doi.org/10.1063/1.1740100.

[47] Li X, Xiao Z, Wu J, Zeng L, Li J, Liu Y, et al. Study on the rapid decompression rate of PA6 liner material of type IV on-board hydrogen storage cylinders. Int J Hydrogen Energy 2024;88:209–27. https://doi.org/10.1016/j.ijhydene.2024.09.183.

[48] Koga A, Uchida K, Yamabe J, Nishimura S. Evaluation on high-pressure hydrogen decompression failure of rubber O-ring using design of experiments. Int J Automot Eng 2011;2:123–9. https://doi.org/10.20485/jsaeijae.2.4_123.
[49] Jaravel J, Castagnet S, Grandidier J-C, Gueguen M. Experimental real-time tracking and diffusion/mechanics numerical simulation of cavitation in gas-saturated elastomers. Int J Solid Struct 2013;50:1314–24. https://doi.org/10.1016/j.ijsolstr.2013.01.001.
[50] Kane-Diallo O, Castagnet S, Nait-Ali A, Benoit G, Grandidier J-C. Time-resolved statistics of cavity fields nucleated in a gas-exposed rubber under variable decompression conditions – support to a relevant modeling framework. Polym Test 2016;51:122–30. https://doi.org/10.1016/j.polymertesting.2016.03.004.
[51] Fujiwara H, Ono H, Ohyama K, Kasai M, Kaneko F, Nishimura S. Hydrogen permeation under high pressure conditions and the destruction of exposed polyethylene-property of polymeric materials for high-pressure hydrogen devices (2)-. Int J Hydrogen Energy 2021;46:11832–48. https://doi.org/10.1016/j.ijhydene.2020.12.223.
[52] Kanehashi S, Nagai K. Analysis of dual-mode model parameters for gas sorption in glassy polymers. J Membr Sci 2005;253:117–38. https://doi.org/10.1016/j.memsci.2005.01.003.
[53] Sato Y, Fujiwara K, Takikawa T, Sumarno Takishima S, Masuoka H. Solubilities and diffusion coefficients of carbon dioxide and nitrogen in polypropylene, high-density polyethylene, and polystyrene under high pressures and temperatures. Fluid Phase Equilib 1999;162:261–76. https://doi.org/10.1016/S0378-3812(99)00217-4.
[54] Zheng D, Li J, Liu B, Yu B, Yang Y, Han D, et al. Molecular dynamics investigations into the hydrogen permeation mechanism of polyethylene pipeline material. J Mol Liq 2022;368:120773. https://doi.org/10.1016/j.molliq.2022.120773.
[55] Melnichuk M, Gardavaud Q, Thiébaud F, Perreux D. Temperature effect in cavitation risk assessments of polymers for hydrogen systems. Int J Hydrogen Energy 2020;45:23020–6. https://doi.org/10.1016/j.ijhydene.2020.05.224.